Optics Letters

Carrier envelope offset detection via simultaneous supercontinuum and second-harmonic generation in a silicon nitride waveguide

Yoshitomo Okawachi,[1,*] Mengjie Yu,[1,2] Jaime Cardenas,[3,4] Xingchen Ji,[2,3] Alexander Klenner,[1] Michal Lipson,[3] and Alexander L. Gaeta[1]

[1]Department of Applied Physics and Applied Mathematics, Columbia University, New York, New York 10027, USA
[2]School of Electrical and Computer Engineering, Cornell University, Ithaca, New York 14853, USA
[3]Department of Electrical Engineering, Columbia University, New York, New York 10027, USA
[4]Currently at The Institute of Optics, University of Rochester, Rochester, New York 14627, USA
*Corresponding author: y.okawachi@columbia.edu

Received 3 July 2018; revised 21 August 2018; accepted 22 August 2018; posted 22 August 2018 (Doc. ID 337681); published 19 September 2018

We demonstrate a chip-scale $f-2f$ interferometer for carrier-envelope-offset frequency (f_{CEO}) detection. This is enabled by simultaneously producing octave-spanning coherent supercontinuum generation and second-harmonic generation in a single dispersion-engineered silicon nitride waveguide. We measure the f_{CEO} beatnote of an 80 MHz modelocked pump source with a signal-to-noise ratio of 25 dB. Our simple approach for $f-2f$ interferometry enables a straightforward route towards a chip-scale self-referenced frequency comb source that can operate at low pulse energies.

https://doi.org/10.1364/OL.43.004627

The development of fully stabilized optical frequency combs has been crucial for high-precision frequency measurements and has led to advances in wide areas of research, including time and frequency metrology, optical clocks, and spectroscopy. Many of the comb sources rely on stabilizing the repetition rate and carrier-envelope offset frequency f_{CEO} of a modelocked femtosecond laser. The f_{CEO} can be detected using a self-referencing technique based on an $f-2f$ interferometer [1,2], which requires an octave-spanning coherent spectrum via supercontinuum generation (SCG) in a nonlinear medium, such as photonic crystal fiber [3]. Recently, there has been tremendous development of complementary metal-oxide-semiconductor (CMOS) process compatible, chip-based photonic platforms for SCG [4–22]. The high optical confinement and nonlinear index in these devices yield a large effective nonlinearity, enabling SCG with moderate pump powers.

Silicon nitride (Si_3N_4) has been shown to be an ideal nonlinear platform for SCG on-chip, largely due to the high nonlinear index ($n_2 = 2.5 \times 10^{-19}$ m^2/W), low linear losses in the near-infrared [23,24], and the ability to engineer the dispersion of the waveguide [25]; f_{CEO} detection [11,19] and stabilization [13,17] have been performed. However, $f-2f$ interferometry is performed off-chip using bulk optics and a periodically poled lithium niobate (PPLN) crystal. Simultaneous generation of SCG and second-harmonic generation (SHG) have been shown with 6 nJ pulse energies in a PPLN waveguide [26] and with 800 pJ pulse energies in an aluminum nitride waveguide [18], due to the strong second-order nonlinear ($\chi^{(2)}$) effect. Alternatively, Carlson, *et al.* [17] have shown direct $f-3f$ interferometry using third-harmonic generation and dispersive wave (DW) formation in the silicon nitride waveguide, which required 1.1 nJ of pulse energy in the waveguide.

In this Letter, we demonstrate direct $f-2f$ interferometry and f_{CEO} detection via simultaneous SCG and SHG in a single Si_3N_4 waveguide with sub-100 pJ pulses. We theoretically investigate the waveguide geometry that allows for SHG which spectrally overlaps with the generated supercontinuum (SC) spectrum and show experimentally an octave-spanning SCG that spectrally overlaps with the SHG signal. We measure an f_{CEO} beat with 27 dB signal-to-noise ratio (SNR) using 62 pJ of pulse energy in the waveguide. Our scheme greatly reduces the complexity of f_{CEO} detection interferometry and is a significant step towards chip-scale integration of a stabilized frequency comb source.

While Si_3N_4 is a centrosymmetric material, it has been previously shown to exhibit a $\chi^{(2)}$ response that can be used to produce SHG and sum frequency generation (SFG) with modest efficiency. This is attributed possibly to symmetry breaking at the waveguide interface [27,28] or to the high film stress induced in Si_3N_4 during the deposition process [29,30]. To achieve efficient SHG in the Si_3N_4 waveguide, we consider the phase-matching conditions by determining when the effective index of the TE_0 mode at the fundamental wavelength is equal to that of a higher-order mode at the second-harmonic

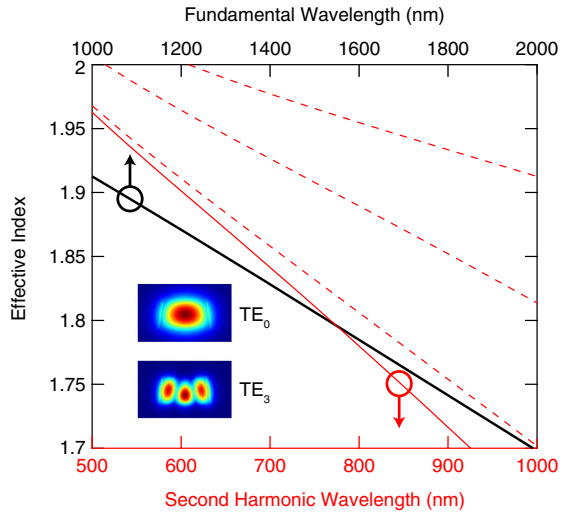

Fig. 1. Simulated effective refractive indices of the TE modes for the fundamental and second harmonic in a Si_3N_4 waveguide with a cross section of 725 × 1400 nm and a 9° sidewall angle. The black curve corresponds to the effective index of the TE_0 mode at the fundamental wavelengths. The red curves correspond to the effective index of the lowest to the fourth-order modes at the second-harmonic wavelengths. The solid red curve corresponds to the fourth-order TE mode, TE_3. Inset: mode profile of fundamental mode (top) and fourth-order mode (bottom) at the crossing point.

wavelength [27,31–34]. Figure 1 shows the effective index for the first 4 TE modes at the fundamental and second-harmonic wavelengths in a Si_3N_4 waveguide with a cross section of 725 × 1400 nm. The black curve corresponds to the fundamental TE mode for the fundamental wavelengths, and the red curves correspond to the first four TE modes at the second-harmonic wavelengths. The plot indicates that the effective indices of the fundamental TE mode and fourth-order TE mode matches at a second-harmonic wavelength near 770 nm.

Next, to determine the conditions for which the SC spectrum can spectrally overlap with the second-harmonic signal, we model the pulse propagation dynamics by solving the nonlinear envelope equation using the split-step Fourier method [35] which includes the effects of third-order nonlinearity, higher-order dispersion, and self-steepening. We assume 200 fs input pulses centered at 1510 nm with 62 pJ of pulse energy. The waveguide is a 2 cm long oxide-clad Si_3N_4 waveguide with a cross section of 725 × 1400 nm. We take advantage of DW formation to extend the SC bandwidth toward the lower wavelengths. The spectral position where the DWs form can be accurately predicted using the dispersion function D [3,19]:

$$D = \sum_{n=2,3,\ldots} \frac{\beta_n(\omega_0)}{n!}(\omega - \omega_0)^n, \tag{1}$$

where β_n corresponds to the nth-order dispersion coefficient, and ω_0 is the pump frequency. DW formation occurs when the dispersion function is near zero. Figure 2(a) shows the dispersion function for a pump at 1510 nm and predicts a DW near 600 nm. The simulated SC spectrum is shown in Fig. 2(b) and is characterized by a DW centered at 640 nm.

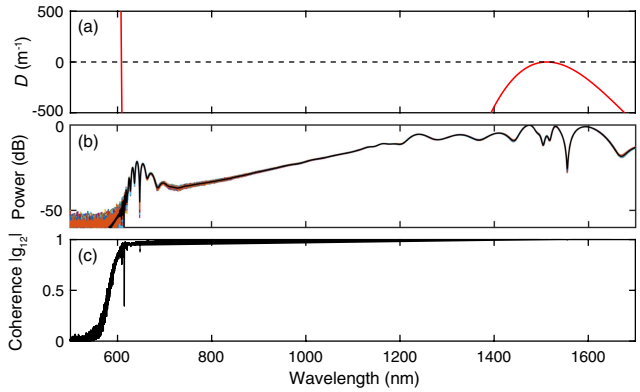

Fig. 2. Dispersion and SCG simulation in a 2 cm Si_3N_4 waveguide with a cross section of 725 × 1400 nm. (a) Dispersion function D predicts the position of the DW for a 1510 nm pump. (b) Simulated spectrum with 200 fs pules and 62 pJ pulse energy in the waveguide. (c) Calculated first-order mutual coherence.

Furthermore, our spectrum shows good spectral overlap with the second-harmonic component. We characterize the spectral coherence by calculating the first-order mutual coherence g_{12} [12,36,37]. Our calculations indicate that the SC spectrum exhibits near unity coherence over the entire bandwidth.

In our experiment, we pump a 2 cm long oxide-clad Si_3N_4 waveguide using 200 fs pulses from a femtosecond optical parametric oscillator (OPO) centered at 1510 nm with a repetition rate of 80 MHz. We estimate a coupling loss of 7 dB and a propagation loss of 0.6 dB/cm. First, we investigate the SHG bandwidth in our waveguide. The output of the waveguide is collected using a lensed fiber and sent to an optical spectrum analyzer. We verify that there are no additional

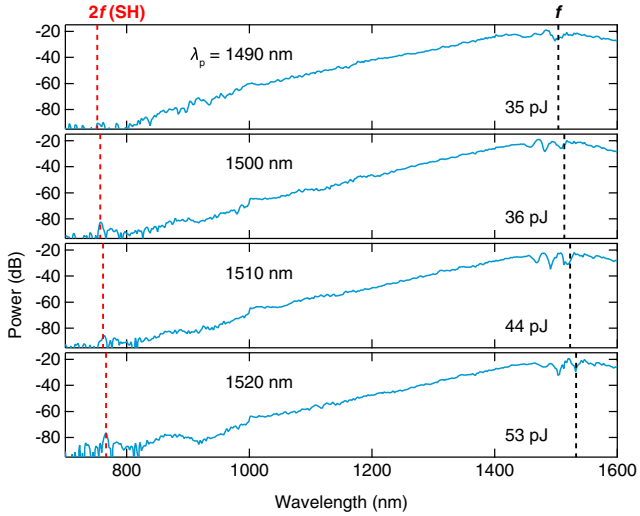

Fig. 3. Experimental spectra showing SHG for pump wavelengths from 1490 to 1530 nm in 10 nm steps. The second-harmonic wavelength and the corresponding fundamental wavelength are denoted with dashed red and black lines, respectively. The discontinuity in the spectrum at 1 μm corresponds to a difference in noise floor due to a detector switching within the optical spectrum analyzer. The pulse energies in the waveguide are indicated on the plot.

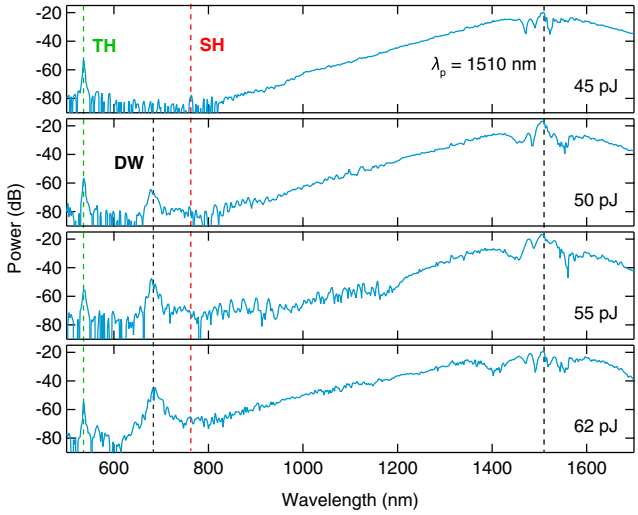

Fig. 4. Measured SCG spectra as the pulse energy in the waveguide is increased from 45 to 62 pJ (top to bottom). A DW is generated at 677 nm. The pump wavelength is 1510 nm. The positions of the second harmonic and third harmonic are labeled SH and TH, respectively.

nonlinear effects in the collection fiber by reducing the output coupling efficiency in the lensed fiber. Figure 3 shows the generated second-harmonic signal for different OPO center wavelengths in the range of 1490–1520 nm, in 10 nm steps. The second-harmonic wavelength and the corresponding fundamental wavelength are shown with red and black dashed lines, respectively. A measurable second-harmonic signal is generated between 752 and 762 nm, corresponding to fundamental wavelengths between 1504 and 1524 nm. In each of the spectra, we also observe a weak signal near 784 nm which we believe corresponds to the ideal phase-matching position. The dynamics underlying the SHG and SFG process are under further investigation. The pulse energy in the waveguide is denoted on the plot. As the pump wavelength is increased, the spectral broadening towards the blue is reduced, and more pump power is required. Taking into account the SHG bandwidth and the power required to broaden the spectrum via SCG, we choose a pump wavelength of 1510 nm.

Next, we look at the generated spectrum for various pump powers. Figure 4 shows the measured SCG spectra as the pump power is increased. The pulse energy in the waveguide is denoted on the plot. We observe the onset of SHG at 762 nm with 45 pJ (Fig. 4, top). We also observe a peak at 536 nm which we attribute to third-harmonic generation or third-order SFG. With 50 pJ, we observe DW formation centered at 677 nm. With a further increase in pump power, spectral components near the $2f$ wavelength increase and, at 62 pJ (Fig. 4, bottom), we observe a continuous SC spectrum down to 600 nm.

Finally, to detect the f_{CEO}, we filter the generated spectrum using an optical short-pass filter (900 nm cutoff wavelength) and send it to a silicon avalanche photodetector with a 1 GHz response. The beatnote is measured using an RF spectrum analyzer for two different pump wavelengths, 1460 and 1510 nm. The measured output pulse energy is 46 pJ for both cases, and Fig. 5 shows the optical and RF spectra for both pump wavelengths. For a 1460 nm pump, the phase-matching conditions for SHG are not satisfied, and the second harmonic is not generated. Thus, in the RF domain, we only observe the repetition frequency f_{rep} at 80 MHz and its harmonics. For a 1510 nm pump, we observe broad SCG, and the RF spectrum shows an f_{CEO} beatnote with an SNR of 27 dB at 100 kHz resolution bandwidth. The achievable SNR may be limited by the temporal walk-off and the spatial overlap between the f and $2f$ components [17]. The SNR can be further increased by optimizing the waveguide design to increase the spectral power of the SC near the SHG wavelength. Furthermore, our scheme can be implemented at other pump wavelengths by adjusting the waveguide cross section to allow for tuning the SHG phase matching and DW position.

In conclusion, we demonstrate on-chip $f-2f$ interferometry by simultaneous SCG and SHG in a single Si_3N_4 waveguide. We measure the f_{CEO} beatnote with 25 dB SNR using 62 pJ of pulse energy. The low power consumption and simplicity of the scheme offer promise as a step towards the realization of a fully integrated stabilized frequency comb source that is compact and portable for applications outside of the laboratory environment.

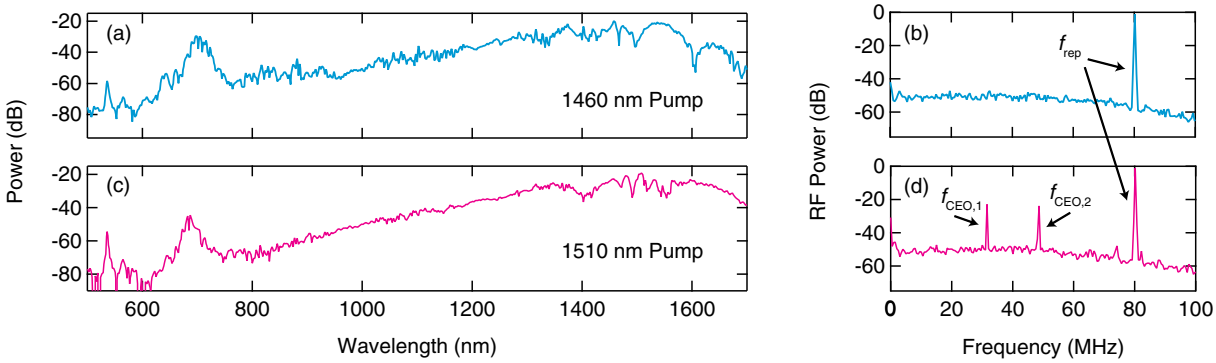

Fig. 5. Measured SC spectra pumped at (a) 1460 and (c) 1510 nm. (b) and (d) show the corresponding RF spectra. While spectrally similar, a 1460 nm pump does not allow for the second harmonic, and only the repetition frequency f_{rep} at 80 MHz and its harmonic appear (b). For a 1510 nm pump, we measure a strong f_{CEO} beatnote with an SNR of 27 dB at 100 kHz resolution bandwidth.

Funding. Defense Advanced Research Projects Agency (DARPA) (N66001-16-1-4055); Air Force Office of Scientific Research (AFOSR) (FA9550-15-1-0303); National Science Foundation (NSF) (ECS-0335765).

Acknowledgment. This Letter was performed in part at the Cornell Nano-Scale Facility, which is a member of the National Nanotechnology Infrastructure Network, supported by the NSF, and at the CUNY Advanced Science Research Center NanoFabrication Facility.

REFERENCES

1. H. R. Telle, G. Steinmeyer, A. E. Dunlop, J. Stenger, D. H. Sutter, and U. Keller, Appl. Phys. B **69**, 327 (1999).
2. S. A. Diddams, D. J. Jones, J. Ye, S. T. Cundiff, J. L. Hall, J. K. Ranka, R. S. Windeler, R. Holzwarth, T. Udem, and T. W. Hänsch, Phys. Rev. Lett. **84**, 5102 (2000).
3. J. M. Dudley, G. Genty, and S. Coen, Rev. Mod. Phys. **78**, 1135 (2006).
4. B. Kuyken, X. Liu, R. M. Osgood, Y. A. Vlasov, R. Baets, G. Roelkens, and W. M. Green, Opt. Express **19**, 20172 (2011).
5. D. Duchesne, M. Peccianti, M. R. Lamont, M. Ferrera, L. Razzari, F. Légaré, R. Morandotti, S. Chu, B. E. Little, and D. J. Moss, Opt. Express **18**, 923 (2010).
6. R. Halir, Y. Okawachi, J. S. Levy, M. A. Foster, M. Lipson, and A. L. Gaeta, Opt. Lett. **37**, 1685 (2012).
7. J. P. Epping, T. Hellwig, M. Hoekman, R. Mateman, A. Leinse, R. G. Heideman, A. van Rees, P. J. M. van der Slot, C. J. Lee, C. Fallnich, and K.-J. Boller, Opt. Express **23**, 19596 (2015).
8. R. K. W. Lau, M. R. E. Lamont, A. Griffith, Y. Okawachi, M. Lipson, and A. L. Gaeta, Opt. Lett. **39**, 4518 (2014).
9. F. Leo, J. Safioui, B. Kuyken, G. Roelkens, and S.-P. Gorza, Opt. Express **22**, 28997 (2014).
10. B. Kuyken, T. Ideguchi, S. Holzner, M. Yan, T. W. Hänsch, J. V. Campenhout, P. Verheyen, S. Coen, F. Leo, R. Baets, G. Roelkens, and N. Picqué, Nat. Commun. **6**, 6310 (2015).
11. A. S. Mayer, A. R. Johnson, A. Klenner, K. Luke, M. R. E. Lamont, Y. Okawachi, M. Lipson, U. Keller, and A. L. Gaeta, Opt. Express **23**, 15440 (2015).
12. A. R. Johnson, A. S. Mayer, A. Klenner, K. Luke, E. S. Lamb, M. R. E. Lamont, C. Joshi, Y. Okawachi, F. W. Wise, M. Lipson, U. Keller, and A. L. Gaeta, Opt. Lett. **40**, 5117 (2015).
13. A. Klenner, A. S. Mayer, A. R. Johnson, K. Luke, M. R. E. Lamont, Y. Okawachi, M. Lipson, A. L. Gaeta, and U. Keller, Opt. Express **24**, 11043 (2016).
14. X. Liu, M. Pu, B. Zhou, C. J. Krückel, A. Fülöp, V. Torres-Company, and M. Bache, Opt. Lett. **41**, 2719 (2016).
15. D. Y. Oh, K. Y. Yang, C. Fredrick, G. Ycas, S. A. Diddams, and K. J. Vahala, Nat. Commun. **8**, 13922 (2017).
16. M. A. G. Porcel, F. Schepers, J. P. Epping, T. Hellwig, M. Hoekman, R. G. Heideman, P. J. M. van der Slot, C. J. Lee, R. Schmidt, R. Bratschitsch, C. Fallnich, and K.-J. Boller, Opt. Express **25**, 1542 (2017).
17. D. R. Carlson, D. D. Hickstein, A. Lind, S. Droste, D. Westly, N. Nader, I. Coddington, N. R. Newbury, K. Srinivasan, S. A. Diddams, and S. B. Papp, Opt. Lett. **42**, 2314 (2017).
18. D. D. Hickstein, H. Jung, D. R. Carlson, A. Lind, I. Coddington, K. Srinivasan, G. G. Ycas, D. C. Cole, A. Kowligy, C. Fredrick, S. Droste, E. S. Lamb, N. R. Newbury, H. X. Tang, S. A. Diddams, and S. B. Papp, Phys. Rev. Appl. **8**, 014025 (2017).
19. Y. Okawachi, M. Yu, J. Cardenas, X. Ji, M. Lipson, and A. L. Gaeta, Opt. Lett. **42**, 4466 (2017).
20. N. Singh, M. Xin, D. Vermeulen, K. Shtyrkova, N. Li, P. T. Callahan, E. S. Magden, A. Ruocco, N. Fahrenkopf, C. Baiocco, B. P.-P. Kuo, S. Radic, E. Ippen, F. X. Kärtner, and M. R. Watts, Light Sci. Appl. **7**, 17131 (2018).
21. H. Guo, C. Herkommer, A. Billat, D. Grassani, C. Zhang, W. Weng, M. H. P. Pfeiffer, C.-S. Brés, and T. J. Kippenberg, Nat. Photonics **12**, 330 (2018).
22. M. Sinobad, C. Monat, B. Luther-Davies, P. Ma, S. Madden, D. J. Moss, A. Mitchell, D. Allioux, R. Orobtchouk, S. Boutami, J.-M. Hartmann, J.-M. Fedeli, and C. Grillet, Optica **5**, 360 (2018).
23. Y. Xuan, Y. Liu, L. T. Varghese, A. J. Metcalf, X. Xue, P.-H. Wang, K. Han, J. A. Jaramillo-Villegas, A. A. Noman, C. Wang, S. Kim, M. Teng, Y. J. Lee, B. Niu, L. Fan, J. Wang, D. E. Leaird, A. M. Weiner, and M. Qi, Optica **3**, 1171 (2016).
24. X. Ji, F. A. S. Barbosa, S. P. Roberts, A. Dutt, J. Cardenas, Y. Okawachi, A. Bryant, A. L. Gaeta, and M. Lipson, Optica **4**, 619 (2017).
25. A. C. Turner, C. Manolatou, B. S. Schmidt, M. Lipson, M. A. Foster, J. E. Sharping, and A. L. Gaeta, Opt. Express **14**, 4357 (2006).
26. C. Langrock, M. M. Fejer, I. Hartl, and M. E. Fermann, Opt. Lett. **32**, 2478 (2007).
27. J. S. Levy, M. A. Foster, A. L. Gaeta, and M. Lipson, Opt. Express **19**, 11415 (2011).
28. A. Billat, D. Grassani, M. H. P. Pfeiffer, S. Kharitonov, T. J. Kippenberg, and C.-S. Brés, Nat. Commun. **8**, 1016 (2017).
29. K. Luke, A. Dutt, C. B. Poitras, and M. Lipson, Opt. Express **21**, 22829 (2013).
30. J. B. Khurgin, T. H. Stievater, M. W. Pruessner, and W. S. Rabinovich, J. Opt. Soc. Am. B **32**, 2494 (2015).
31. J. K. Ranka, R. S. Windeler, and A. J. Stentz, Opt. Lett. **25**, 796 (2000).
32. F. G. Omenetto, A. J. Taylor, M. D. Moores, J. Arriaga, J. C. Knight, W. J. Wadsworth, and P. S. J. Russell, Opt. Lett. **26**, 1158 (2001).
33. S. Miller, K. Luke, Y. Okawachi, J. Cardenas, A. L. Gaeta, and M. Lipson, Opt. Express **22**, 26517 (2014).
34. X. Xue, F. Leo, Y. Xuan, J. A. Jaramillo-Villegas, P.-H. Wang, D. E. Leard, M. Erkintalo, M. Qi, and A. M. Weiner, Light Sci. Appl. **6**, e16253 (2017).
35. A. L. Gaeta, Opt. Lett. **27**, 924 (2002).
36. X. Gu, M. Kimmel, A. P. Shreenath, R. Trebino, J. M. Dudley, S. Coen, and R. S. Windeler, Opt. Express **11**, 2697 (2003).
37. A. Ruehl, M. J. Martin, K. C. Cossel, L. Chen, H. McKay, B. Thomas, C. Benko, L. Dong, J. M. Dudley, M. E. Fermann, I. Hartl, and J. Ye, Phys. Rev. A **84**, 011806(R) (2011).